Electrical Power and Energy Systems 141 (2022) 108087

Contents lists available at ScienceDirect

International Journal of Electrical Power and Energy Systems

journal homepage: www.elsevier.com/locate/ijepes

A model-less control algorithm of DC microgrids based on feedback optimization

J. Carlos Olives-Camps, Álvaro Rodríguez del Nozal, Juan Manuel Mauricio, José María Maza-Ortega *

Department of Electrical Engineering, Universidad de Sevilla, Camino de los descubrimientos s/n, Seville, 41092, Spain

ARTICLE INFO

Keywords:
DC microgrids
Distributed control
Feedback optimization
Load sharing control
Secondary voltage control

ABSTRACT

This work addresses the problem of the optimal real-time control of a DC microgrid without relying on its corresponding network model. The main goal of such a controller is to keep the nodal network voltages within the regulatory limits while offering current sharing capability between the different controllable generators powering the DC microgrid. The proposed model-less methodology is based on feedback optimization, which takes advantage of the available real-time measurements to update the setpoints of the DC generation assets. The optimal control variables are determined in an iterative manner by applying a primal–dual saddle-point method, which guarantees appropriate convergence features. The paper details both centralized and distributed implementations which are compared through simulations. The results evidence a good dynamic performance and an optimal steady-state operation as the proposed control algorithm converges to the solution provided by a conventional model-based Optimal Power Flow.

1. Introduction

Electrification of small power systems in remote locations without a straightforward access to a power network has traditionally relied on fossil fuel resources [1]. Fortunately, the evolution of all technologies enabling renewable energies has allowed alternative ecofriendly solutions which are feasible from a techno-economic point of view. In fact, the microgrid (MG) concept emerges in 2002 as an integration of different technologies able to supply electrical energy [2]. Basically, a MG is a cluster of at least one renewable energy source, energy storage devices and loads operating as a single controllable system [3].

MGs can be based on AC, DC, or hybrid AC/DC configurations depending on the type of power sources and loads to be interconnected. With this regard, it has to be considered that AC MGs have been extensively studied due to the widespread use of AC loads [4–7]. It is important to highlight, however, the growing importance of DC devices such as photovoltaic (PV) arrays, fuel cell units, battery energy storage systems (BESS), electric vehicles (EV), consumer electronics, variable-frequency drives or LED lighting systems among others. The connection of all these devices to an AC system requires adequate AC/DC interfaces in charge of the power transfer management. Therefore, in those cases with a majority presence of DC devices, DC MGs may constitute an efficient alternative due to the reduction and simplification of power converters [8].

One of the main concerns of the DC MG operation involving several distributed generators (DGs) is to simultaneously achieve an adequate load sharing among them and voltage control within the regulatory limits [9]. In this way, the loads are energized close to their rated voltage with an equitable demand distribution among the DGs to avoid overloads. Therefore, current sharing allows reducing the current injections of some generation units that, without implementing this strategy, would be forced to inject higher currents due to their proximity to the loads or the network topology. As a result, current sharing strategies prevent the oversizing of generation units which leads to lower investments and a higher utilization of the existing assets. Traditionally, the well-known primary droop-based control has been applied to DC MGs to improve stability and offer current sharing capabilities [10,11]. It has been reported, however, that the performance of voltage-based droop methods is unsatisfactory due to the voltage drop caused by the virtual impedance [12]. Several approaches have been presented to improve that behavior, such as nonlinear droop control scheme [13,14], logarithmic droop-based control [15] or piece-wise linear droop function [16]. Although these methods improve the operation with respect to the conventional droop-based techniques, it is still observed a poor performance in case of heavy load conditions.

The incorporation of a secondary controller relying on a communication system solves the problem of voltage deviation guaranteeing

* Corresponding author.
E-mail address: jmmaza@us.es (J.M. Maza-Ortega).

https://doi.org/10.1016/j.ijepes.2022.108087
Received 2 December 2021; Received in revised form 26 January 2022; Accepted 18 February 2022
Available online 17 March 2022

the fulfillment of regulatory voltage limits [17]. Following this trend, a centralized controller computing adequate reference voltages to DGs based on a MG field measurements has been proposed in [18,19]. The main advantage of these centralized approaches is that voltage and power regulation can be formulated as an optimization problem providing optimal results. The main drawback of these methods, however, is that a complete and detailed MG model is required. This approach involves static data, e.g. MG network parameters, and real-time data, e.g. network topology and measurements from the generation and load sides, which are not always available [20,21]. In addition, centralized approaches strongly depend on a communication system which, as any other MG component, may fail.

For all these reasons, distributed methods emerged as an alternative of centralized approaches improving the reliability and resiliency in case of the communication system failure [22]. One of the most used scheme is the communication among neighbors where distributed control based on consensus has gained great popularity [23–26]. Probably, one of the main advantages of the consensus-based approach, in addition to its reduced failure probability compared to centralized schemes, is that a network model is not required. Therefore, the scalability of this type of solutions is higher than those relying on a centralized controller. A comprehensive review of the existing distributed methodologies for DC MGs can be found in [27,28]. In spite of these benefits, it has to be considered that the system performance in terms of convergence rate and dynamic oscillations strongly rely on the communication topology and local control parameters due to the absence of any network model information. For this reason, the main drawback of the distributed approaches is related to the difficulty of properly tuning these control algorithm parameters to achieve an optimal solution.

This paper proposes a compromise solution between the previously analyzed centralized and distributed control algorithms aimed at obtaining voltage control and adequate power sharing among DGs. The proposed approach is based on the feedback optimization (FO) technique [29], which has been successfully applied to solve the voltage regulation of distribution AC networks by means of reactive power injections [30]. The FO technique uses the real-time system output measurements to iteratively update the DG setpoints, leading the system to the solution of a constrained optimization problem. The setpoint update in this iterative process requires just a reduced model information, i.e. input–output system sensitivity, rather than a complete and accurate system model. The proposed algorithm based on the FO technique is formulated both for centralized and distributed implementations and compared with the solution of an Optimal Power Flow (OPF).

The remainder of this paper is organized as follows. Section 2 presents a formal description of the problem under analysis and a mathematical model of the problem in its simplest version. In Section 3, the concept of FO is stated and the assumptions to design and implement the controller for DC MGs are introduced. The performance of the method is tested under simulation in Section 4. Finally, the main conclusions and future research are outlined in Section 5.

2. Problem formulation

Let us consider a DC MG comprising a set of buses $\mathcal{V}_g$ which are interconnected by a set of power lines $\mathcal{E}_g$. Part of the buses, $\mathcal{V} = \{1, \dots, n\} \subseteq \mathcal{V}_g$, are powered by primary energy sources or energy storage systems interfaced with controllable power electronic devices. In the sequel, it will be assumed that these devices within $\mathcal{V}$ have capability to set the bus voltage to a given reference value and, therefore, can be considered as DC grid-former devices. These devices are also equipped with a communication interface for the required information exchange. The voltage and current injection of the DC grid-former device connected to the node $k \in \mathcal{V}$ are denoted as v_k and i_k, respectively. The rest of the nodes within the DC MG, $\mathcal{V}_g \backslash \mathcal{V}$, are generation or load nodes without these advanced control and communication capabilities. Therefore, the devices connected to the nodes $l \in \mathcal{V}_g \backslash \mathcal{V}$ can be characterized by their corresponding non-controllable power injections p_l.

The goals of the set of controllable devices connected to $\mathcal{V}$ are to simultaneously: (i) control their corresponding nodal voltages, v_k, with respect to their setpoints, $v_k^\star$; (ii) share as much as possible the load to avoid any overloading. These objectives can be achieved by solving a constrained optimization problem with the following objective function and constraints for each controllable node $k \in \mathcal{V}$:

- Objective function. It is composed of the voltage deviation and current sharing terms, $C_k^v(v_k)$ and $C_{k,j}^i(i_k, i_j)$ respectively, weighted through the parameters β_k and $\gamma_{k,j}$ as follows:

$$J_k(v_k, i_k, i_j) = \beta_k C_k^v(v_k) + \sum_{j \in \mathcal{N}_k} \gamma_{k,j} C_{k,j}^i(i_k, i_j), \tag{1}$$

  The voltage deviation term is computed as the squared difference between the actual and reference voltages:

$$C_k^v(v_k) = (v_k - v_k^\star)^2. \tag{2}$$

  Similarly, the current sharing term between the grid-former devices connected to nodes k and j is formulated as the squared difference of their injected currents:

$$C_{k,j}^i(i_k, i_j) = (i_k - i_j)^2. \tag{3}$$

  In this respect, note that the current sharing terms within (1) are extended just to the set of nodes $\mathcal{N}_k$ which are adjacent to the considered k node in order to facilitate a decentralized implementation of this optimization problem.
- Inequality constraints. Voltage and current at the controllable nodes must be within the regulatory limits and the rated current of each grid-former device, respectively:

$$\underline{v}_k \le v_k \le \overline{v}_k, \qquad \forall k \in \mathcal{V}, \tag{4}$$

$$-\overline{i}_k \le i_k \le \overline{i}_k, \qquad \forall k \in \mathcal{V}. \tag{5}$$

- Equality constraints. Eqs. (1) and (5) are formulated as a function of the current injections of the controllable grid-former devices i_k. These currents are dependent variables of the controllable grid-former voltages, v_k ($k \in \mathcal{V}$), the non-controllable power injections, p_l ($l \in \mathcal{V}_g \backslash \mathcal{V}$) as well as the topology and parameters of the DC network. This dependency can be mathematically formulated as:

$$\mathbf{i} = \mathbf{h}(\mathbf{v}, \mathbf{w}), \tag{6}$$

  where $\mathbf{i} = \text{col}(i_k)$ and $\mathbf{v} = \text{col}(v_k)$ are column vectors that stack the current injections and nodal voltages at controllable buses $k \in \mathcal{V}$, while $\mathbf{w} = \text{col}(p_l)$ is a vector that contains the power injections in the non-controllable nodes $l \in \mathcal{V}_g \backslash \mathcal{V}$.

Thus, the setpoint of each controllable grid-former device connected to any bus $k \in \mathcal{V}$, v_k, within the DC MG can be determined by the following constrained optimization problem:

$$\tilde{v}_k = \arg \min_{v_k} \sum_k J_k(v_k, i_k, i_j) \tag{7}$$

$$s.t \ (4), (5), (6).$$

The objective of the proposed problem is twofold. First, voltage deviations from the reference values are penalized. Second, the difference between the current injections of the grid-forming devices are minimized. Note that both objectives are counterbalanced since the lower the value of the first objective, i.e. similar nodal voltages, the greater will be the second, i.e. reduced current sharing between the grid-former devices. Thus, a compromise between both goals can be achieved by adequately tuning the weighting parameters β_k and $\gamma_{k,j}$.

Note that solving the proposed optimization problem without relying on the network model is not trivial, since, although the grid-forming

current injections are measured, it is required to provide adequate and coordinated voltage references to these devices to achieve the pursued current sharing.

This optimization problem can be solved by applying either a centralized or a distributed approach as discussed in the next section.

3. Proposed method

This section presents a feedback optimization (FO) based approach to solve (7). First, some fundamentals of the FO technique are outlined highlighting their main advantages. Then, the centralized and distributed implementations of the FO approach are detailed.

3.1. Fundamentals of FO

The basic objective of any optimization method is to determine the values of the input variables $\mathbf{u}$ within a given actuation range $\mathcal{U}$ that minimize a cost function $f(\mathbf{u},\mathbf{y})$, where $\mathbf{y}$ represents the output signals. The problem can be subject to some constraints on these output signals $\mathbf{y}$ whose values are given by a nonlinear mapping $\mathbf{y}=\mathbf{h}(\mathbf{u},\mathbf{w})$, where $\mathbf{w}$ are uncontrollable variables. In addition, the output signals $\mathbf{y}$ can be constrained by a set of inequalities $\mathbf{g}(\mathbf{y}) \leq \mathbf{0}$. The mathematical formulation of this problem is as follows:

$$\begin{aligned} &\min_{\mathbf{u}\in\mathcal{U}} \; f(\mathbf{u},\mathbf{y}),\\ &s.t. \;\; \mathbf{y}=\mathbf{h}(\mathbf{u},\mathbf{w}),\\ &\quad\;\; \mathbf{g}(\mathbf{y}) \leq \mathbf{0}. \end{aligned}$$

Traditionally, this problem can be solved by relying on its dual formulation through the Lagrangian. However, the augmented Lagrangian can be used instead to improve the convergence rate of the optimization problem, [31]:

$$\begin{aligned} \mathcal{L}(\mathbf{u},\mathbf{w},\boldsymbol{\mu},\mathbf{s}) \;=\; & f(\mathbf{u},\mathbf{h}(\mathbf{u},\mathbf{w})) + \boldsymbol{\mu}^{\top}\left(\mathbf{g}\left(\mathbf{h}(\mathbf{u},\mathbf{w})\right)+\mathbf{s}\right)\\ & + \frac{\rho}{2}\left\|\mathbf{g}\left(\mathbf{h}(\mathbf{u},\mathbf{w})\right)+\mathbf{s}\right\|_2^2, \end{aligned}$$

where the output vector $\mathbf{y}$ has been replaced by the nonlinear mapping $\mathbf{y}=\mathbf{h}(\mathbf{u},\mathbf{w})$ and the slack vector $\mathbf{s}$ has been included to transform the inequality constraint $\mathbf{g}(\mathbf{y}) \leq 0$ into $\mathbf{g}(\mathbf{y})+\mathbf{s}=0$ with $\mathbf{s}\geq 0$.

One of the possible approaches for solving this problem is to apply the well-known primal–dual saddle-point algorithm [32] which is an iterative strategy consisting of a positive and negative gradient flow of dual and primal variables respectively. To implement this algorithm, three main steps are followed: (i) slack variables $\mathbf{s}$ are updated in such a way that the augmented Lagrangian is minimized; (ii) primal variables $\mathbf{u}$ are updated following a gradient descent direction ensuring that $\mathbf{u} \in \mathcal{U}$; (iii) dual variables are updated following a gradient ascent direction. Note that the steps described above need a complete mathematical formulation of the augmented Lagrangian which implies an accurate description of the nonlinear mapping $\mathbf{y}=\mathbf{h}(\mathbf{u},\mathbf{w})$ as well as the information about non-controllable variables $\mathbf{w}$ that are rarely available.

The feedback optimization approach solves this drawback by applying the input variables $\mathbf{u}$ to the physical system and directly measuring the output variables $\mathbf{y}$ instead of estimating them based on an inaccurate or incomplete model. Thus, the mathematical formulation of the *mth* iteration applying the FO approach can be formulated as:

(i) Slack variables $\mathbf{s}$ are updated based on the output measurements $\mathbf{y}(m)$ in such a way that the augmented Lagrangian is minimized:

$$\frac{\partial\mathcal{L}(\mathbf{u}(m),\mathbf{y}(m),\boldsymbol{\mu}(m),\mathbf{s})}{\partial\mathbf{s}} = 0 \Rightarrow \mathbf{s}(m+1) = \left[-\frac{1}{\rho}\boldsymbol{\mu}(m) - \mathbf{g}\left(\mathbf{y}(m)\right)\right]_+,$$

where $[a]_+$ stands for $max(0,a)$.

(ii) Primal variables $\mathbf{u}$ are updated following a negative gradient flow:

$$\mathbf{u}(m+1) = \mathbf{u}(m) - \alpha\frac{\partial\mathcal{L}(\mathbf{u},\mathbf{y}(m),\boldsymbol{\mu}(m),\mathbf{s}(m+1))}{\partial\mathbf{u}},$$

where α is the algorithm step size. If the new value of primal variables $\mathbf{u}(m+1)\notin\mathcal{U}$, then the value of $\mathbf{u}(m+1)$ is modified to that projected into set $\mathcal{U}$. Note that to compute the augmented Lagrangian derivative, $\partial\mathcal{L}/\partial\mathbf{u}$, the system model is not required but just the information about the sensitivities of the output variables $\mathbf{y}$ with respect to the input vector $\mathbf{u}$.

(iii) Input variables $\mathbf{u}(m+1)$ are applied to the system and the output variables $\mathbf{y}(m+1)$ are measured. Finally, the value of the dual variables are updated by following a positive gradient flow:

$$\boldsymbol{\mu}(m+1) = \boldsymbol{\mu}(m) + \rho\left[\mathbf{g}(\mathbf{y}(m+1)) + \mathbf{s}(m+1)\right].$$

As a result, the optimization problem, in case of applying the outlined FO approach, can be solved without the system model, $\mathbf{h}$, and without the measurements of the exogenous uncontrollable variables, $\mathbf{w}$.

3.2. Centralized implementation

This section presents a centralized implementation to solve (7) in which a central controller computes the setpoints of the grid-former devices based on their nodal voltages and current injections, v_k and i_k.

First, the objective function of the centralized problem, $J(\mathbf{v},\mathbf{i})$, is formulated by aggregating all the individual cost functions $J_k(v_k,i_k,i_j)$ related to the grid-former devices. This objective function can be expressed in a matrix form as:

$$J(\mathbf{v},\mathbf{i}) = \left(\mathbf{v}-\mathbf{v}^{\star}\right)^{\top}\mathbf{Q}\left(\mathbf{v}-\mathbf{v}^{\star}\right) + \mathbf{i}^{\top}\mathbf{A}\mathbf{R}\mathbf{A}^{\top}\mathbf{i} \tag{8}$$

where $\mathbf{v}^{\star}$ is a column vector with the voltage references of all the devices, $\mathbf{Q}$ is a diagonal matrix with the weighting factors used for penalizing the voltage deviations, $\mathbf{A}$ is the incidence matrix relating nodes and branches, and $\mathbf{R}$ is a diagonal matrix with the weighting factors used for penalizing the current differences. An explanatory example clarifying how to build these matrices can be found in Appendix.

Once the objective function has been formulated, constraints (4) and (5) can be written in terms of input and output variables, $\mathbf{v}$ and $\mathbf{i}$, as follows:

$$\mathbf{v}\in\mathcal{U}, \quad \mathbf{C}\mathbf{i}\leq\mathbf{d}, \tag{9}$$

where $\mathbf{C}$ is a block diagonal matrix composed by terms $\mathbf{C}_k$ and $\mathbf{d}$ is a column vector described by terms $\mathbf{d}_k$ which are formally defined in Appendix.

Therefore, the centralized optimization problem can be formulated in a compact form as:

$$\begin{aligned} \tilde{\mathbf{v}} \;=\; & \arg\min_{\mathbf{v}} J(\mathbf{v},\mathbf{i}) \\ s.t. \;\; & \mathbf{C}\mathbf{i}\leq\mathbf{d}\\ & \mathbf{v}\in\mathcal{U}, \end{aligned} \tag{10}$$

whose augmented Lagrangian is constructed as:

$$\begin{aligned} \mathcal{L}(\mathbf{v},\mathbf{w},\boldsymbol{\mu},\mathbf{s}) \;=\; & J(\mathbf{v},\mathbf{h}(\mathbf{v},\mathbf{w})) + \boldsymbol{\mu}^{\top}\left(\mathbf{C}\mathbf{h}(\mathbf{v},\mathbf{w})-\mathbf{d}+\mathbf{s}\right)\\ & + \frac{\rho}{2}\left\|\mathbf{C}\mathbf{h}(\mathbf{v},\mathbf{w})-\mathbf{d}+\mathbf{s}\right\|_2^2, \end{aligned} \tag{11}$$

where $\mathbf{i}$ has been substituted by (6) to formulate the problem in terms of $\mathbf{v}$.

The solution of (10) can be done by applying the FO technique described in the previous section consisting on the following steps which have been particularized for the *mth* iteration:

(i) The slack vector $\mathbf{s}$ is updated to minimize the augmented Lagrangian (11):

Table 1
Iterative algorithm for the centralized approach.

Iterative algorithm	
Initialization:	
1:	Set β_k and $\gamma_{k,j}$ for every $k \in \mathcal{V}$ and $j \in \mathcal{N}_k$.
2:	Set $v_k = 1$ p.u. for every $k \in \mathcal{V}$ and dispatch to the grid-forming devices.
3:	Set $\boldsymbol{\mu} = 0$ and $\mathbf{s} = 0$.
4:	Compute sensitivity matrix $\mathbf{H}$.
Iterative update:	
5:	Compute $\mathbf{s}$ according to (12).
6:	Compute $\tilde{\mathbf{v}}$ according to (13).
7:	Dispatch $\tilde{v}_k$ to the grid-forming devices.
8:	Collect the measurements of $\mathbf{i}$.
9:	Update the value of $\boldsymbol{\mu}$ using (14).

$$\frac{\partial \mathcal{L}(\mathbf{v}(m), \mathbf{w}(m), \boldsymbol{\mu}(m), \mathbf{s})}{\partial \mathbf{s}} = 0 \Rightarrow \mathbf{s}(m) = \left[-\frac{1}{\rho}\boldsymbol{\mu}(m) - \mathbf{C}\mathbf{i}(m) - \mathbf{d} \right]_+ . \tag{12}$$

(ii) The decision vector $\mathbf{v}$ is updated by following a gradient descent flow:

$$\mathbf{v}(m+1) = \mathbf{v}(m) - \alpha \frac{\partial \mathcal{L}(\mathbf{v}, \mathbf{w}(m), \boldsymbol{\mu}(m), \mathbf{s}(m+1))}{\partial \mathbf{v}}, \tag{13}$$

where, relying on matrix differentiation properties, it is possible to formulate the augmented Lagrangian sensitivities with respect to the input variables as:

$$\begin{aligned}\frac{\partial \mathcal{L}(\mathbf{v}, \mathbf{w}(m), \boldsymbol{\mu}(m), \mathbf{s}(m+1))}{\partial \mathbf{v}} &= 2\mathbf{Q}(\mathbf{v}(m) - \mathbf{v}^\star) + 2\mathbf{H}^\top \mathbf{A}\mathbf{R}\mathbf{A}^\top \mathbf{i}(m) \\ &+ \mathbf{H}^\top \mathbf{C}^\top \left[\boldsymbol{\mu}(m) + \rho(\mathbf{C}\mathbf{i}(m) - \mathbf{d} + \mathbf{s}(m+1)) \right],\end{aligned}$$

being $\mathbf{H}$ the sensitivity matrix of the output variables $\mathbf{i}$ with respect to the input signals $\mathbf{v}$.

(i) The computed voltage setpoints $\mathbf{v}(m+1)$ are dispatched to the grid-forming devices and the current injections $\mathbf{i}(m+1)$ are measured and sent to the central controller once the steady-state regime has been reached. Note that due to the fast dynamic response of the power electronic devices, the transient response is expected to be quite short. Finally, the measurement of the injected currents are used to update the dual variables by following a gradient ascent direction:

$$\boldsymbol{\mu}(m+1) = \boldsymbol{\mu}(m) + \rho \left[\mathbf{C}\mathbf{i}(m+1) - \mathbf{d} + \mathbf{s}(m+1) \right]. \tag{14}$$

These steps are iteratively repeated according to the algorithm summarized in Table 1 until the convergence to the optimal solution is achieved.

Finally, it is important to note that the sensitivity matrix $\mathbf{H}$ is not constant as the $\mathbf{h}(\mathbf{v}, \mathbf{w})$ is a nonlinear function. Different methods to estimate this matrix can be used, e.g. considering a linear approximation of the power flow equations [33] or applying a perturb-and-observe method [34], being the latter used in this work. A detailed explanation of the procedure followed to estimate the sensitivity matrix, along with an explanatory example, is specified in Appendix. Moreover, the effect of inaccurate estimations of $\mathbf{H}$ is discussed in Section 4.

3.3. Distributed solution

This section proposes a distributed implementation approach to solve (7) as an alternative to the centralized methodology presented in the previous section. In this case, the optimization problem is solved in a distributed manner taking advantage of the computation and communication capabilities within the controllable generation units. The objective function related to the *kth* grid-forming device can be formulated as:

$$J_k(v_k, \mathbf{i}) = \beta_k (v_k - v_k^\star)^2 + \mathbf{i}^\top \mathbf{A}\mathbf{R}_k \mathbf{A}^\top \mathbf{i}, \tag{15}$$

where $\mathbf{R}_k$ is a diagonal matrix, formally specified in the Appendix, that contains the weighting factors used for penalizing the current differences of the grid-forming device k with respect to their adjacent ones. On the other hand, the constraints (4) and (6) are transformed to:

$$v_k \in \mathcal{U}_k, \quad \mathbf{C}_k i_k \leq \mathbf{d}_k$$

where $\mathbf{C}_k$ is the kth diagonal block of matrix $\mathbf{C}$ and $\mathbf{d}_k$ is the kth block of column vector $\mathbf{d}$. The augmented Lagrangian considering these objective function and constraints can be formulated as:

$$\begin{aligned}\mathcal{L}_k(\mathbf{v}, \mathbf{w}, \boldsymbol{\mu}_k, \mathbf{s}_k) &= J_k(v_k, \mathbf{h}(\mathbf{v}, \mathbf{w})) + \boldsymbol{\mu}_k^\top \left(\mathbf{C}_k [\mathbf{h}(\mathbf{v}, \mathbf{w})]_k - \mathbf{d}_k + \mathbf{s}_k \right) \\ &+ \frac{\rho}{2} \left\| \mathbf{C}_k [\mathbf{h}(\mathbf{v}, \mathbf{w})]_k - \mathbf{d}_k + \mathbf{s}_k \right\|_2^2 .\end{aligned}$$

Then, it is a simple matter to check that the following equality is fulfilled:

$$\mathcal{L}(\mathbf{v}, \mathbf{w}, \boldsymbol{\mu}, \mathbf{s}) = \sum_{k \in \mathcal{V}} \mathcal{L}_k(\mathbf{v}, \mathbf{w}, \boldsymbol{\mu}_k, \mathbf{s}_k)$$

where $\mathcal{L}(\mathbf{v}, \mathbf{w}, \boldsymbol{\mu}, \mathbf{s})$ is the Lagrangian of centralized problem (10). Therefore, the solution of the distributed implementation will be exactly the same that the one of the centralized problem if each *kth* grid-forming device computes its voltage v_k according to:

$$\sum_{j \in \mathcal{V}} \frac{\partial \mathcal{L}_j(\mathbf{v}, \mathbf{w}, \boldsymbol{\mu}_j, \mathbf{s}_j)}{\partial v_k} = 0,$$

with

$$\frac{\partial \mathcal{L}_j(\mathbf{v}, \mathbf{w}, \boldsymbol{\mu}_j, \mathbf{s}_j)}{\partial v_k} = \frac{\partial J_j(v_j, \mathbf{i})}{\partial v_k} + h_{j,k} \mathbf{C}_j^\top \left(\boldsymbol{\mu}_j + \rho(\mathbf{C}_j i_j - \mathbf{d}_j + \mathbf{s}_j) \right), \tag{16}$$

being

$$\begin{aligned}\frac{\partial J_k(v_k, \mathbf{i})}{\partial v_k} &= 2\beta_k (v_k - v_k^\star) + 2\mathbf{H}_k^\top \mathbf{A}\mathbf{R}_k \mathbf{A}^\top \mathbf{i}, \\ \frac{\partial J_j(v_j, \mathbf{i})}{\partial v_k} &= 2\mathbf{H}_j^\top \mathbf{A}\mathbf{R}_j \mathbf{A}^\top \mathbf{i},\end{aligned}$$

where $\mathbf{H}_j$ and $h_{j,k}$ are the jth column and j, k element of the sensitivity matrix $\mathbf{H}$ respectively. Note that the inspection of (16) indicates the information that must be shared by the controllable units in this distributed approach. With this regard, (16) has two terms corresponding to the objective function and constraints respectively. On the one hand, the constraint term has to be considered just when $h_{j,k} \neq 0$, as it is multiplied by this sensitivity, which only happens in case of being the controllable nodes j and k adjacent each other. On the other hand, and regarding the objective function terms, note that $J_j(v_k, \mathbf{i})$ includes only the currents injected by the adjacent controllable devices as shown in (1). These currents, in turn, depend on the voltages of their corresponding adjacent nodes. Therefore, the term $J_j(v_k, \mathbf{i})$ must be considered just in case the nodes j and k are separated less or equal to two hops being its value null otherwise. As a result, all the controllable devices must share: (i) its injected current i_k with other controllable sources within 2 hops and (ii) the Lagrange multipliers and slack variables, $\boldsymbol{\mu}_j$ and $\mathbf{s}_j$, with other controllable sources within 1 hop. It is worth pointing out that an undirected communication network is used to exchange all the required information among the grid-forming devices. Therefore the information flows in both directions between each pair of controllable grid-forming devices. Nevertheless, and for clarification purposes, an explanatory example has been included in Appendix.

The primal–dual saddle-point algorithm is particularized to the distributed approach as follows:

(i) The slack vector $\mathbf{s}_k$ of each controllable grid-former device is updated in such a way that the local augmented Lagrangian is minimized:

$$\mathbf{s}_k(m+1) = \left[-\frac{1}{\rho}\boldsymbol{\mu}_k(m) - \mathbf{C}_k \mathbf{i}(m) + \mathbf{d} \right]_+ . \tag{17}$$

Table 2
Iterative algorithm for the distributed approach.

Iterative algorithm	
Initialization:	
1:	Set β_k and $\gamma_{k,j}$ for every $k \in \mathcal{V}$ and $j \in \mathcal{N}_k$.
2:	Set $v_k = 1$ p.u. for every $k \in \mathcal{V}$ and dispatch to the grid-forming devices.
3:	Set $\boldsymbol{\mu}_k = 0$ and $\mathbf{s}_k = 0$.
4:	Compute sensitivities $\mathbf{H}_k$ for every $k \in \mathcal{V}$.
5:	Exchange $\mathbf{R}_k$ and $\mathbf{H}_k$ with those nodes separated less or equal to two hops form k.
Iterative update:	
6:	Compute $\mathbf{s}_k$ according to (17).
7:	Compute $\bar{v}_k$ according to (18).
8:	Apply input signal $\bar{v}_k$ to the real system.
9:	Measure i_k and exchange it with the neighboring devices.
10:	Update the value of $\boldsymbol{\mu}_k$ using (19).
11:	Exchange $\boldsymbol{\mu}_k$ and $\mathbf{s}_k$ with the neighboring devices.

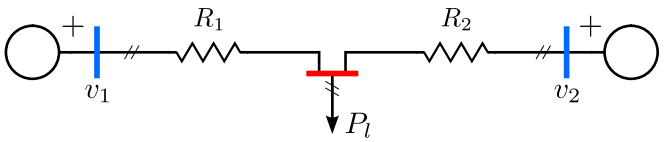

Fig. 1. One-line diagram of the simple test case.

(ii) The voltage v_k is updated in each grid-former device as follows:

$$v_k(m+1) = v_k(m) - \alpha \sum_{j \in \mathcal{V}} \frac{\partial \mathcal{L}_j(\mathbf{v}, \mathbf{w}(m), \boldsymbol{\mu}_j(m), \mathbf{s}_j(m+1))}{\partial v_k}, \tag{18}$$

where terms $\partial \mathcal{L}_j(\mathbf{v}, \mathbf{w}, \boldsymbol{\mu}_j, \mathbf{s}_j)/\partial v_k$ have been previously defined in (16).

(iii) The already computed voltage $v_k(m+1)$ is set in each grid-forming device and the current injections $i_k(m+1)$ are measured and exchanged with the 2-hop neighboring generation units and used to update the Lagrange multipliers as:

$$\boldsymbol{\mu}_k(m+1) = \boldsymbol{\mu}_k(m) + \rho \left[\mathbf{C}_k i_k(m+1) - \mathbf{d}_k + \mathbf{s}_k(m+1)\right], \tag{19}$$

Once computed, the Lagrange multipliers along with the slack variables, $\boldsymbol{\mu}_k(m+1)$ and $\mathbf{s}_k(m+1)$, are shared with the 1-hop neighboring controllable grid-forming converters.

The method is iteratively repeated until the convergence has been reached. The main steps of the distributed approach presented in this section can be found in Table 2.

4. Performance assessment

This section provides the performance assessment of the centralized and distributed implementations of the proposed algorithm in two DC MGs. First, some explanatory examples are presented in a simple network conformed by two grid-former devices supplying a load. Second, a larger DC MG composed by 38 buses with 7 grid-former devices is used to evidence the good performance and scalability of the proposed methodology.

4.1. Simple test case

The simple test bench considered in this subsection is depicted in Fig. 1, where the grid-former devices are connected to buses 1 and 2 while the load is connected to a node in between of them. The main network parameters are listed in Table 3. It is assumed that the grid-former devices have identical rated power with reference voltages equal to the network rated voltage and, to evidence the dynamic performance of the methodology, the load doubles its power demand at $t = 4.5$ s. This simple network will allow to analyze the influence

Table 3
Parameters of the simple test case.

Parameter	Value
Rated dc voltage	380 V
R_1 line resistance	0.0844 Ω
R_2 line resistance	0.2110 Ω
P_l dc load	25 kW
Communication period	0.02 s

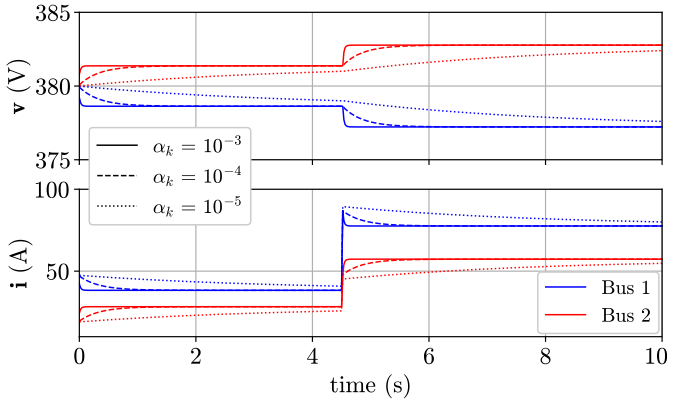

Fig. 2. Influence of parameter α in the convergence rate of the algorithm ($\beta_k = 100.0$ and $\gamma_{k,j} = 1.0$).

of the algorithm parameters, i.e. the weighting factors of the objective function and sensitivity matrix, which has been implemented in its centralized version. In addition, it will be checked the current sharing and voltage regulation capabilities in case of high-load conditions. In this regard, note that the resistance between one grid-former device and the load is different than the other one. Thus, it should be possible to compare the suitability of the proposed method with the conventional droop control [4].

4.1.1. Influence of the algorithm parameters

This section analyzes the effect of parameters α, β_k and $\gamma_{k,j}$ on the convergence rate and steady-state solution of the proposed algorithm.

First, Fig. 2 shows the influence of the parameter α in the convergence rate of the algorithm. Parameter α is used in the second step of the algorithm to update the primal variables (13). Since primal variables are directly applied to the grid-forming devices as voltage setpoints, larger values of α imply larger variations in the control signals and, consequently, faster convergence is achieved. Note that this parameter only affects the convergence rate of the method, reaching the same steady-state solution in all the cases.

Fig. 3 evaluates the effect of changing the ratio between the weighting factors used within the cost function (1). Particularly, it depicts the voltages and currents evolution for $\beta_k = 100$ and different values of $\gamma_{k,j}$. Note that the higher $\gamma_{k,j}$ the better current sharing capability at the cost of a larger voltage deviation with respect to the reference value. On the contrary, nodal voltages are slightly deviated from their reference value when $\gamma_{k,j}$ takes lower values but to the detriment of the load sharing between the grid-former devices. Thus, the tuning of these weighting parameters makes it possible to achieve a required compromise between both counterbalanced objectives.

4.1.2. Influence of sensitivity errors

As stated in Section 3, the FO technique exclusively relies on the sensitivity of the injected currents with respect to the controlled voltages. Therefore, it is neither required an in-depth knowledge of the power flows in the system nor an accurate grid model. For the estimation of this sensitivity matrix, this work proposes the use of a

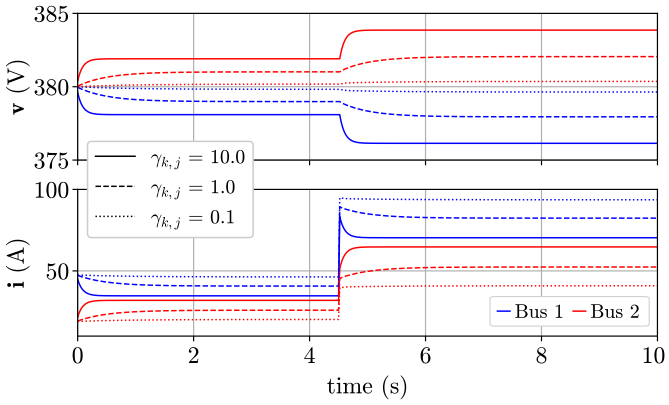

Fig. 3. Influence of the weighting factors ($\alpha = 0.0001$, $\beta_k = 100$): $\gamma_{k,j} = 10, 1, 0.1$.

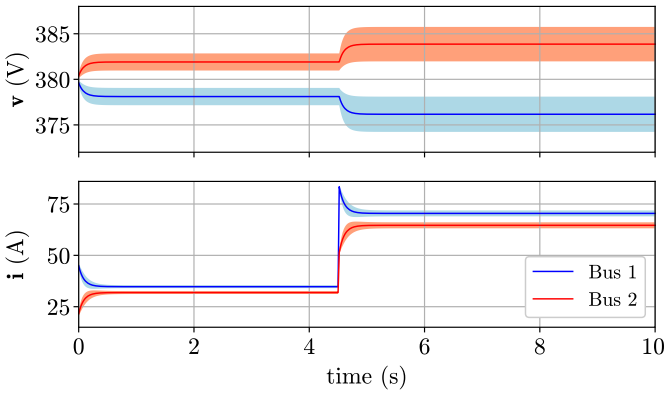

Fig. 4. Influence of the errors on the estimation of the sensitivity matrix ($\alpha = 0.0001$, $\gamma_{k,j} = 10$, $\beta_j = 100$).

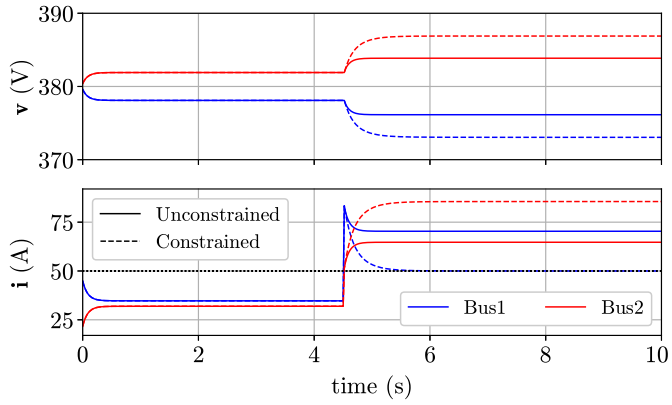

Fig. 5. Evolution of voltages and current injections for the unconstrained and constrained scenarios (current constraint $\bar{i}_1 = 50\,\text{A}$) ($\alpha = 0.0001$, $\gamma_{k,j} = 10$, $\beta_j = 100$).

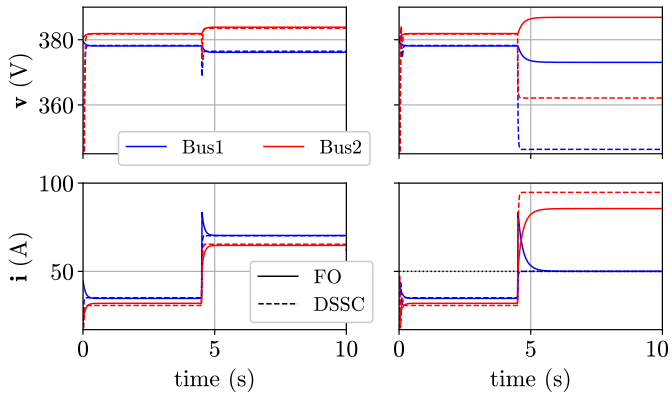

Fig. 6. Evolution of voltages and current injections. Left: unconstrained scenario. Right: current constraint ($\bar{i}_1 = 50\,\text{A}$). FO stands for the proposed approach and DSSC for that presented in [35] ($\alpha = 0.0001, \beta_k = 100$ and $\gamma_{k,j} = 10$).

perturb-and-observe method. Its application, however, may lead to estimation errors on the sensitivity matrix which may affect the algorithm performance. In order to assess this influence, five hundred simulations with measurement errors both in the perturbed and observed magnitudes have been carried out. The errors are characterized by a normal distribution with zero mean and standard deviations of 10% and 30% for the applied voltages and current injections, i.e., perturbations and observed magnitudes, respectively. As a result, five hundred different sensitivity matrices have been obtained which lead to different algorithm performances. These simulations are depicted within Fig. 4 where $\beta_k = 100$ and $\gamma_{k,j} = 10$. The solid lines denote the evolution of the voltage and current mean values, while the shadowed area represents the envelope of the evolution of these magnitudes for the 99.7% of the simulated cases. Note that the voltage and the current sharing deviations are within bands of 0.58% and 3.60% respectively. Therefore, it is possible to conclude that the algorithm is robust to errors in the estimation of the sensitivity matrix.

4.1.3. Performance with constrained variables

Now, the dynamic performance of the algorithm when current or voltage constraints are violated is evaluated. The results are depicted in Fig. 5 where an unconstrained scenario has been included for comparison purposes. The constrained scenario evaluates the algorithm performance when a current limit $\bar{i}_1 = 50\,\text{A}$ is imposed to the grid-former device connected at bus 1 (black dotted line). Note that after the step change in the load, this current limit is overpassed. Consequently, the control algorithm starts decreasing the current contribution of the corresponding grid-former device to fulfill this constraint, whereas the other controllable generator starts increasing its current to supply the load.

4.1.4. Comparison with similar approaches

Finally, the proposed method is compared with the one presented in [35], where a secondary regulation of the network is introduced by means of two independent controllers in charge of voltage regulation and current sharing respectively. Using that approach instead of a linear combination of both, the performance of the control strategy is improved getting rid of coupling effects. A supervisory device switches between both control laws based on the information collected by local sensors. However, this strategy does not take into account constraints in the problem, such as voltage or current limitations, which are considered in the approach proposed in this paper. Fig. 6 compares the performance of both approaches. In the left side, the evolution of voltages and currents for the unconstrained scenario is shown. As it can be seen, both methods behave similarly converging to almost the same steady-state solution. In the right side of the figure it is shown the evolution of the same magnitudes but with the constrained scenario (maximum current of the grid-forming device at bus 1 set to 50 A). Since the approach presented in [35] does not take into consideration operational constraints, the current output of that grid-forming device has been limited in the simulation. As a consequence, the device at bus 2 increases its current injection to cover the load. However, unlike the approach presented in this paper, the nodal voltages of both buses decrease considerably.

4.2. Application to a larger dc system

In this section, the scalability of the proposed method is evaluated on a larger system. In particular, the simulations are conducted on a DC

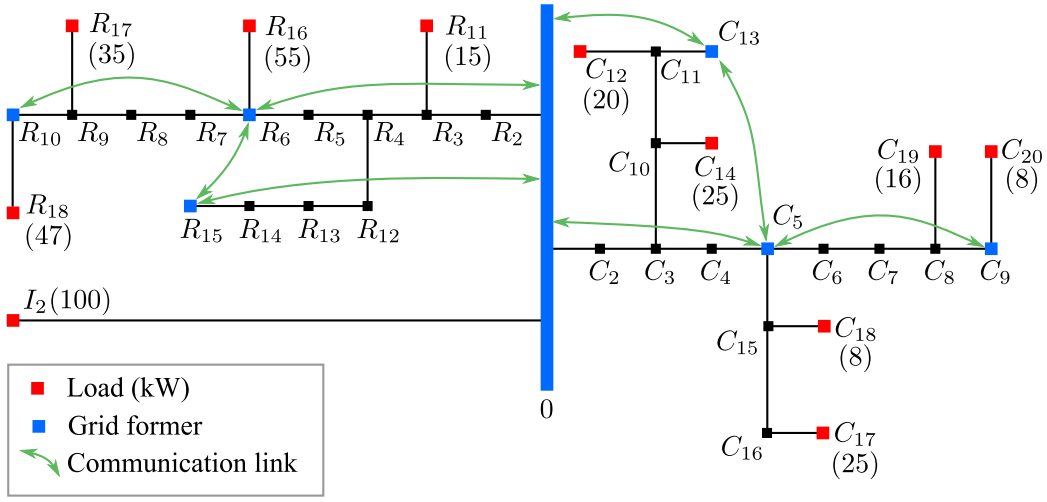

Fig. 7. DC microgrid based on the CIGRE European LV benchmark distribution network including the communication infrastructure (green lines).

MG which has been adapted from the CIGRE European LV benchmark distribution network [36]. The system topology and bus names remain unaltered, as shown in Fig. 7 where the one-line diagram is represented, but the network parameters have been accordingly modified for a DC supply. Buses 0, R_6, R_{10}, R_{15}, C_5, C_9, and C_{13} (blue buses) are endowed with grid-former devices with a voltage reference of 380 V. Fig. 7 shows also the required undirected communication links between these devices in the case of a distributed implementation of the proposed FO control technique. For both centralized and distributed schemes, the communication period is 100 ms. Loads (red buses) are connected to nodes $R11$, $R16$, $R17$, $R18$, $C12$, $C14$, $C17$, $C18$, $C19$, $C20$ and $I2$ with the power demands in kW detailed within brackets.

Furthermore, to test the dynamical response of the method, two events are considered. First, an uncontrolled distributed generator is connected to the bus R_{18} at $t = 5$ s, transforming the net consumption of 47 kW to an excess of generation of 5 kW. Second, an additional load of 40 kW is connected to bus I_2 at $t = 10$ s.

Centralized (solid lines) and distributed (green lines) implementations have been simulated with the results shown in Fig. 8. Particularly, the evolution of the voltages and currents of the controllable devices are detailed and compared with the results of a classical OPF (dotted lines). In addition, it has been included a third plot representing the difference of the nodal voltages at the controllable buses for centralized and distributed implementations. As it can be seen, both centralized and distributed approaches converge to the same result in steady state being only slightly different during transient periods. As expected, the centralized approach converges faster to the optimal solution because it operates with global information. In addition, both strategies converge to the OPF solution, i.e. achieving the optimal solution.

Finally, Fig. 9 represents a comparison of the distributed approach when one of the grid-forming devices loses its communication capability. In particular, a communication failure is considered in the grid-forming device connected to the bus R15 at $t = 8$ s, when the steady state has been reached after the first load change. At this point, this device keeps its output voltage constant, which leads to a lack of injected current when the load increase at $t = 10$ s occurs, which has been represented as the orange shaded area in Fig. 9. As a result of this system malfunction, the rest of the grid-forming devices increase their corresponding current injection to compensate this generation deficit.

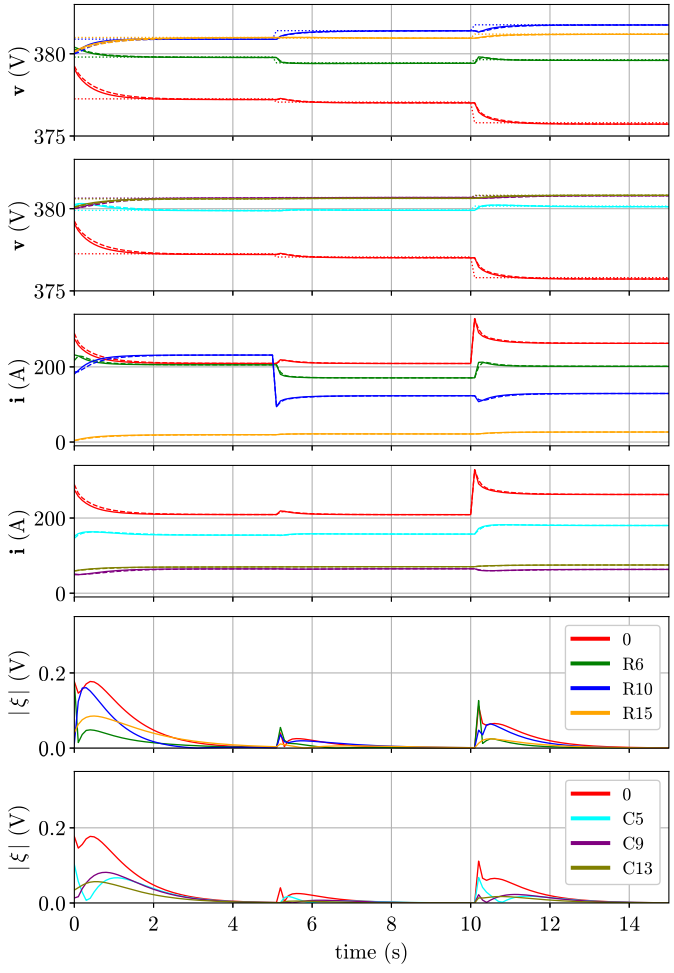

Fig. 8. Simulation results for the larger-scale system when implementing the proposed centralized approach (solid lines), the distributed approach (dashed lines) and a classical offline OPF (dotted lines). ξ stands for the difference between centralized and distributed control actions.

5. Conclusion

This paper has presented a real-time control methodology for DC MGs supplied by a set of controllable grid-forming devices. The methodology is based on Feedback Optimization (FO), which is able to solve an optimization problem subject to a set of constraints without requiring a precise system model. Particularly, an objective function including

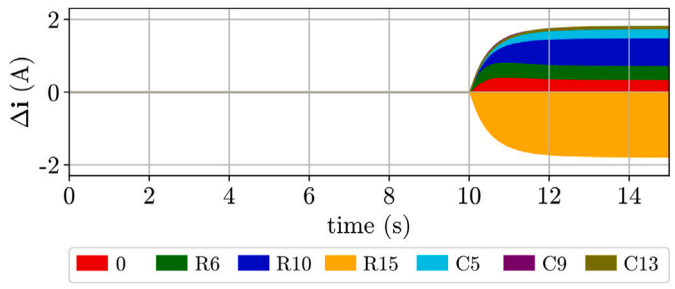

Fig. 9. Simulation results for the larger-scale system comparing the injected currents by grid-forming devices for normal operation and a communication failure of the grid-former device in R15.

voltage regulation and current sharing between the controllable grid-forming devices has been used along with operational constraints dealing with voltage limits and rated currents of the controllable generation.

The main advantages of the proposed FO technique to solve the posed constrained optimization problem can be summarized as follows. First, the solving procedure does not require a complete system model to compute the optimal solution but just the sensitivity matrix of the injected currents by the controllable generation units with respect to the voltages. Second, the FO technique can be applied following either a centralized or a distributed implementation. In the former case, each grid-forming controllable device shares its local information with a central controller in charge of solving the optimization problem and dispatching the optimal voltage setpoints. Conversely, the distributed approach solves in a distributed manner exactly the same optimization problem. For this purpose, it is required to share information between the controllable grid-forming devices. Nevertheless, it is worth mentioning that the distributed implementation significantly reduces the communication requirements. With this regard, note that each controllable unit just requires the local information of the adjacent devices within 2-hop distance.

The paper has included two test cases to evidence the good performance of the FO technique. First, the simple test with just two controllable units and a load has proven the good dynamic response of the centralized approach, the influence of the weighting parameters of the objective function, and the capability of the algorithm to cope in a dynamic manner with the operational constraints. In addition, this simple test has evidenced the robustness of the FO technique in case of estimation errors on the sensitivity matrix, probably one of the drawbacks of the methodology. With this regard, even in the case of significant errors on the estimation of this matrix, the obtained optimal solution has a reduced error with respect to its theoretical value. In addition, it has been included an additional test case to show the performance in a larger network with a larger number of controllable units. Both centralized and distributed implementations converge to the OPF solution computed using a full network model. In addition, the dynamic performance of both implementations is quite similar, revealing the high potential that the distributed implementation may have in actual DC MGs due to the lower communication requirements. With this regard, it has been also tested the failure of a communication link of a controllable generation device in order to evidence the performance of the algorithm with this contingency. As expected, the rest of the controllable generation units take over the power mismatch of the failed generation device.

Future research lines dealing with the application of the outlined FO technique in DC MGs will focus on the incorporation of ampacity limits as an additional operational constraint to the optimization problem. Furthermore, the extension of the proposed method to that in which the communication network among the grid-forming devices is defined by a directed graph will be investigated. Additionally, the consideration of new objective functions that optimize economic aspects of the network operation will be studied. Finally, the extension of this real-time control approach to AC networks will be analyzed in future works.

CRediT authorship contribution statement

J. Carlos Olives-Camps: Conceptualization, Methodology, Software, Writing – original draft. **Álvaro Rodríguez del Nozal:** Conceptualization, Software, Writing – original draft. **Juan Manuel Mauricio:** Conceptualization, Writing – review & editing, Supervision, Funding acquisition. **José María Maza-Ortega:** Conceptualization, Writing – review & editing, Supervision, Funding acquisition.

Declaration of competing interest

The authors declare that they have no known competing financial interests or personal relationships that could have appeared to influence the work reported in this paper.

Acknowledgments

This work was supported by Universidad de Sevilla in the framework of VI PPIT-US; by the EASY-RES project that has received funding from European Union's Horizon 2020 Research and Innovation programme under Grant 764090; by the Spanish Ministry of Economy under grant no. ENE2017-84813-R; and by the CERVERA research programme of CDTI, the Industrial and Technological Development Centre of Spain, under the research Project HySGrid+ (CER-20191019).

The authors thank Prof. Xiaokang Liu for his valuable help when reproducing the Distributed Supervisory Secondary Controller used for comparison purposes of the proposed FO methodology.

Appendix A. Formal mathematical formulation

This appendix is devoted to provide a formal mathematical formulation of all the matrices used for the centralized and distributed implementations of the proposed methodology.

The matrix formulation of the centralized approach given by (8) is based on the following matrices for a DC MG comprising m branches and n nodes:

- $\mathbf{Q} = \text{diag}(\beta_k)_{k\in\mathcal{V}}$: voltage weight matrix. It is a diagonal matrix whose diagonal terms are the weighting parameters β_k for every $k \in \mathcal{V}$.
- $\mathbf{A}$: incidence matrix. It is a $n\times m$ matrix that relates nodes and lines in the network. In that way, the matrix elements are defined as:

$$a_{k,l} = \begin{cases} 1 & \text{if the } l\text{th link is incident to but directed away from node } k, \\ -1 & \text{if the } l\text{th link is incident to but directed towards node } k, \\ 0 & \text{if the } l\text{th link is not incident to.} \end{cases}$$

- $\mathbf{R}$: current sharing weight matrix. It is a $m \times m$ which can be computed as:

$$\mathbf{R} = \sum_{k\in\mathcal{V}} \mathbf{R}_k$$

where matrices R_k are $m\times m$ diagonal matrices with the following matrix elements:

$$r_{l,l} = \begin{cases} \gamma_{k,j} & \text{if the } l\text{th line of the DC MG corresponds to that between nodes } k \text{ and } j \\ 0 & \text{otherwise} \end{cases}$$

- $\mathbf{C}$: constraint matrix. It is a block diagonal matrix whose diagonal terms are $\mathbf{C}_k = [1, -1]^\top$ where sub-index k makes reference to the kth block diagonal element of the matrix.

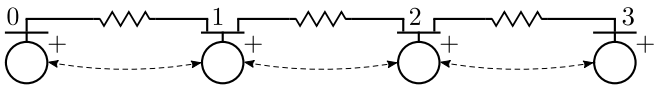

Fig. C.10. Simple 4-bus system with distributed communication layer.

- **d**: constraint vector. It is a column vector conformed by terms $\mathbf{d}_k = [\bar{i}_k, \bar{i}_k]^\top$ where sub-index k refers to each of the k elements of the vector.

Note that the matrix formulation of the distributed implementation is based on the matrices $\mathbf{R}_k$, $\mathbf{C}_k$ and $\mathbf{d}_k$ which has been previously defined.

Appendix B. Sensitivity matrix estimation

The sensitivity matrix **H** defines the influence of the variation of the input variables, i.e. controllable voltages of the grid-forming devices **v**, on the output variables, i.e. current injections of the grid-forming devices **i**. For example, considering the example depicted in Fig. C.10 with four grid-forming devices, the sensitivity matrix can be formulated as:

$$\mathbf{H} = \begin{bmatrix} \frac{\partial i_0}{\partial v_0} & \frac{\partial i_0}{\partial v_1} & \frac{\partial i_0}{\partial v_2} & \frac{\partial i_0}{\partial v_3} \\ \frac{\partial i_1}{\partial v_0} & \frac{\partial i_1}{\partial v_1} & \frac{\partial i_1}{\partial v_2} & \frac{\partial i_1}{\partial v_3} \\ \frac{\partial i_2}{\partial v_0} & \frac{\partial i_2}{\partial v_1} & \frac{\partial i_2}{\partial v_2} & \frac{\partial i_2}{\partial v_3} \\ \frac{\partial i_3}{\partial v_0} & \frac{\partial i_3}{\partial v_1} & \frac{\partial i_3}{\partial v_2} & \frac{\partial i_3}{\partial v_3} \end{bmatrix}.$$

To estimate each of matrix terms, the following steps are required. First, it is assumed that all the grid-forming devices are operating in steady state defined by a set of voltages v_k and currents i_k. Next, a variation in the voltage setpoint of one grid-forming device is performed, e.g. Δv_0 while maintaining the setpoints of the rest. The new current injections are collected and compared with their previous values obtaining the corresponding variations Δi_k. The quotient between current and voltage variations constitute the terms in matrix **H**. This procedure is iteratively repeated for each grid-forming device within the DC MG until all the terms of the sensitivity matrix are obtained.

It is important to highlight that this procedure can be simplified. Note that current injections of devices depend only on voltage variations of neighboring grid-forming devices and the device itself. Thus, for instance, in the example depicted in Fig. C.10, i_0 is only sensitive to variations of v_0 or v_1 being zero otherwise. In that way, the sensitivity terms $\partial i_k/\partial v_j$ for $j \neq k, \mathcal{N}_k$ can be set to zero a priori, being only necessary to compute the rest of the terms of the sensitivity matrix.

Appendix C. Explanatory example

Consider the network example depicted in Fig. C.10 where four grid-forming devices are considered. The decision vector is defined as $\mathbf{v} = [v_0, v_1, v_2, v_3]^\top$ while the output signals are current injections $\mathbf{i} = [i_0, i_1, i_2, i_3]^\top$.

Based on these input and output vectors, the matrices used in the centralized implementation expressed by (8) are:

$$\mathbf{A} = \begin{bmatrix} 1 & 0 & 0 \\ -1 & 1 & 0 \\ 0 & -1 & 1 \\ 0 & 0 & -1 \end{bmatrix}, \mathbf{Q} = \begin{bmatrix} \beta_0 & 0 & 0 & 0 \\ 0 & \beta_1 & 0 & 0 \\ 0 & 0 & \beta_2 & 0 \\ 0 & 0 & 0 & \beta_3 \end{bmatrix}$$

$$\mathbf{R} = \begin{bmatrix} \gamma_{0,1}+\gamma_{1,0} & 0 & 0 \\ 0 & \gamma_{1,2}+\gamma_{2,1} & 0 \\ 0 & 0 & \gamma_{2,3}+\gamma_{3,2} \end{bmatrix}.$$

The current constraints are defined by $\mathbf{Ci} \leq \mathbf{d}$ where

$$\mathbf{C} = \begin{bmatrix} \mathbf{C}_0 & 0 & 0 & 0 \\ 0 & \mathbf{C}_1 & 0 & 0 \\ 0 & 0 & \mathbf{C}_2 & 0 \\ 0 & 0 & 0 & \mathbf{C}_3 \end{bmatrix}, \mathbf{d} = \begin{bmatrix} \mathbf{d}_0 \\ \mathbf{d}_1 \\ \mathbf{d}_2 \\ \mathbf{d}_3 \end{bmatrix},$$

with $\mathbf{C}_k = [1, -1]^\top$ and $\mathbf{d}_k = [\bar{i}_k, \bar{i}_k]^\top$ for every $k \in \{0, 1, 2, 3\}$.

Conversely, the matrices used in the distributed approach formulated by (15) for each grid-forming device are:

$$\mathbf{R}_0 = \begin{bmatrix} \gamma_{0,1} & 0 & 0 \\ 0 & 0 & 0 \\ 0 & 0 & 0 \end{bmatrix}, \mathbf{R}_1 = \begin{bmatrix} \gamma_{1,0} & 0 & 0 \\ 0 & \gamma_{1,2} & 0 \\ 0 & 0 & 0 \end{bmatrix},$$

$$\mathbf{R}_2 = \begin{bmatrix} 0 & 0 & 0 \\ 0 & \gamma_{2,1} & 0 \\ 0 & 0 & \gamma_{2,3} \end{bmatrix}, \mathbf{R}_3 = \begin{bmatrix} 0 & 0 & 0 \\ 0 & 0 & 0 \\ 0 & 0 & \gamma_{3,2} \end{bmatrix},$$

Note that $\mathbf{R} = \mathbf{R}_0 + \mathbf{R}_1 + \mathbf{R}_2 + \mathbf{R}_3$. In addition, the current constraints are included using the previously defined matrices $\mathbf{C}_k$ and $\mathbf{d}_k$. Using these matrices, and for illustration purposes, the optimization problem of the grid-forming controllable devices connected to bus 0 is formulated. Basically, it is required to minimize (15) being required the following derivatives of the Lagrangian functions with respect to the control voltage v_0:

$$\begin{aligned} \frac{\partial \mathcal{L}_0}{\partial v_0} &= 2\beta_0(v_0 - v_0^\star) + 2\gamma_{0,1}(h_{0,0} - h_{1,0})(i_0 - i_1) \\ &\quad + h_{0,0}\mathbf{C}_0^\top \left(\boldsymbol{\mu}_0 + \rho(\mathbf{C}_0 i_0 - \mathbf{d}_0 + \mathbf{s}_0)\right), \\ \frac{\partial \mathcal{L}_1}{\partial v_0} &= 2\gamma_{1,0}(h_{1,0} - h_{0,0})(i_1 - i_0) + 2\gamma_{1,2}h_{1,0}(i_1 - i_2) \\ &\quad + h_{1,0}\mathbf{C}_1^\top \left(\boldsymbol{\mu}_1 + \rho(\mathbf{C}_1 i_1 - \mathbf{d}_1 + \mathbf{s}_1)\right), \\ \frac{\partial \mathcal{L}_2}{\partial v_0} &= -2\gamma_{2,1}h_{1,0}(i_2 - i_1), \\ \frac{\partial \mathcal{L}_3}{\partial v_0} &= 0. \end{aligned}$$

Note that, as previously stated in Section 3.3, since the sensitivity of the nodal voltage v_0 to current injections i_2 and i_3 is equal to zero, it is possible to state that:

- Local constraints of grid-forming devices connected at buses 2 and 3 are not included in the computations of the controllable unit connected at bus 0 since they are not 1-hop adjacent devices.
- Current injection of the controllable unit connected to the bus 3 is not required in the computations of the controllable unit at bus 0 since only the currents of those controllable devices connected within 2-hop adjacent nodes are required.

References

[1] Barnes DF. Effective solutions for rural electrification in developing countries: Lessons from successful programs. Curr Opin Environ Sustain 2011;3(4):260–4. http://dx.doi.org/10.1016/j.cosust.2011.06.001, Energy Systems.

[2] Lasseter RH. MicroGrids. In: 2002 IEEE power engineering society winter meeting. Conference proceedings (Cat. No.02CH37309), Vol. 1. 2002, p. 305–8. http://dx.doi.org/10.1109/PESW.2002.985003.

[3] Hatziargyriou N, Asano H, Iravani R, Marnay C. Microgrids. IEEE Power Energy Mag 2007;5(4):78–94. http://dx.doi.org/10.1109/MPAE.2007.376583.

[4] De Brabandere K, Bolsens B, Van den Keybus J, Woyte A, Driesen J, Belmans R. A voltage and frequency droop control method for parallel inverters. IEEE Trans Power Electron 2007;22(4):1107–15. http://dx.doi.org/10.1109/TPEL.2007.900456.

[5] Rocabert J, Luna A, Blaabjerg F, Rodríguez P. Control of power converters in AC microgrids. IEEE Trans Power Electron 2012;27(11):4734–49. http://dx.doi.org/10.1109/TPEL.2012.2199334.

[6] Olivares DE, Mehrizi-Sani A, Etemadi AH, Cañizares CA, Iravani R, Kazerani M, Hajimiragha AH, Gomis-Bellmunt O, Saeedifard M, Palma-Behnke R, Jiménez-Estévez GA, Hatziargyriou ND. Trends in microgrid control. IEEE Trans Smart Grid 2014;5(4):1905–19. http://dx.doi.org/10.1109/TSG.2013.2295514.

[7] Nikkhajoei H, Iravani R. Steady-state model and power flow analysis of electronically-coupled distributed resource units. IEEE Trans Power Deliv 2007;22(1):721–8. http://dx.doi.org/10.1109/TPWRD.2006.881604.

[8] Kumar D, Zare F, Ghosh A. DC microgrid technology: System architectures, AC grid interfaces, grounding schemes, power quality, communication networks, applications, and standardizations aspects. IEEE Access 2017;5:12230–56. http://dx.doi.org/10.1109/ACCESS.2017.2705914.

[9] Han Y, Li H, Shen P, Coelho EAA, Guerrero JM. Review of active and reactive power sharing strategies in hierarchical controlled microgrids. IEEE Trans Power Electron 2017;32(3):2427–51. http://dx.doi.org/10.1109/TPEL.2016.2569597.

[10] Tahim APN, Pagano DJ, Lenz E, Stramosk V. Modeling and stability analysis of islanded DC microgrids under droop control. IEEE Trans Power Electron 2015;30(8):4597–607. http://dx.doi.org/10.1109/TPEL.2014.2360171.

[11] Liu H, Guo W, Cheng D, Wang Y, Wang M. Stability and bifurcation analysis of DC microgrid with multiple droop control sources and loads. IEEE Trans Power Electron 2021;36(2):2361–72. http://dx.doi.org/10.1109/TPEL.2020.3009192.

[12] Chen X, Shi M, Sun H, Li Y, He H. Distributed cooperative control and stability analysis of multiple DC electric springs in a DC microgrid. IEEE Trans Ind Electron 2018;65(7):5611–22. http://dx.doi.org/10.1109/TIE.2017.2779414.

[13] Khorsandi A, Ashourloo M, Mokhtari H, Iravani R. Automatic droop control for a low voltage DC microgrid. IET Gener Transm Distrib 2016;10(1):41–7. http://dx.doi.org/10.1049/iet-gtd.2014.1228.

[14] Prabhakaran P, Goyal Y, Agarwal V. Novel nonlinear droop control techniques to overcome the load sharing and voltage regulation issues in DC microgrid. IEEE Trans Power Electron 2018;33(5):4477–87. http://dx.doi.org/10.1109/TPEL.2017.2723045.

[15] P. M, M. K, Guerrero J. Logarithmic droop-based decentralized control of parallel converters for accurate current sharing in islanded DC microgrid applications. IET Renew Power Gener 2021;1–15. http://dx.doi.org/10.1049/rpg2.12103.

[16] Lin Y, Xiao W. Novel piecewise linear formation of droop strategy for DC microgrid. IEEE Trans Smart Grid 2019;10(6):6747–55. http://dx.doi.org/10.1109/TSG.2019.2911013.

[17] Guerrero JM, Vasquez JC, Matas J, de Vicuna LG, Castilla M. Hierarchical control of droop-controlled AC and DC microgrids—A general approach toward standardization. IEEE Trans Ind Electron 2011;58(1):158–72. http://dx.doi.org/10.1109/TIE.2010.2066534.

[18] Mudaliyar S, Mishra S. Coordinated voltage control of a grid connected ring DC microgrid with energy hub. IEEE Trans Smart Grid 2019;10(2):1939–48. http://dx.doi.org/10.1109/TSG.2017.2783972.

[19] Setiawan MA, Abu-Siada A, Shahnia F. A new technique for simultaneous load current sharing and voltage regulation in DC microgrids. IEEE Trans Ind Inf 2018;14(4):1403–14. http://dx.doi.org/10.1109/TII.2017.2761914.

[20] Maknouninejad A, Qu Z, Lewis FL, Davoudi A. Optimal, nonlinear, and distributed designs of droop controls for DC microgrids. IEEE Trans Smart Grid 2014;5(5):2508–16. http://dx.doi.org/10.1109/TSG.2014.2325855.

[21] Peyghami S, Mokhtari H, Davari P, Loh PC, Blaabjerg F. On secondary control approaches for voltage regulation in DC microgrids. IEEE Trans Ind Appl 2017;53(5):4855–62. http://dx.doi.org/10.1109/TIA.2017.2704908.

[22] Sayed AH. Adaptive networks. Proc IEEE 2014;102(4):460–97. http://dx.doi.org/10.1109/JPROC.2014.2306253.

[23] Trip S, Cucuzzella M, Cheng X, Scherpen J. Distributed averaging control for voltage regulation and current sharing in DC microgrids. IEEE Control Syst Lett 2019;3(1):174–9. http://dx.doi.org/10.1109/LCSYS.2018.2857559.

[24] Fan B, Guo S, Peng J, Yang Q, Liu W, Liu L. A consensus-based algorithm for power sharing and voltage regulation in DC microgrids. IEEE Trans Ind Inf 2020;16(6):3987–96. http://dx.doi.org/10.1109/TII.2019.2941268.

[25] Prabhakaran P, Goyal Y, Agarwal V. A novel communication-based average voltage regulation scheme for a droop controlled DC microgrid. IEEE Trans Smart Grid 2019;10(2):1250–8. http://dx.doi.org/10.1109/TSG.2017.2761864.

[26] Cucuzzella M, Trip S, De Persis C, Cheng X, Ferrara A, van der Schaft A. A robust consensus algorithm for current sharing and voltage regulation in DC microgrids. IEEE Trans Control Syst Technol 2019;27(4):1583–95. http://dx.doi.org/10.1109/TCST.2018.2834878.

[27] Han Y, Ning X, Yang P, Xu L. Review of power sharing, voltage restoration and stabilization techniques in hierarchical controlled DC microgrids. IEEE Access 2019;7:149202–23. http://dx.doi.org/10.1109/ACCESS.2019.2946706.

[28] Meng L, Dragicevic T, Roldán-Pérez J, Vasquez JC, Guerrero JM. Modeling and sensitivity study of consensus algorithm-based distributed hierarchical control for DC microgrids. IEEE Trans Smart Grid 2016;7(3):1504–15. http://dx.doi.org/10.1109/TSG.2015.2422714.

[29] Häberle V, Hauswirth A, Ortmann L, Bolognani S, Dörfler F. Non-convex feedback optimization with input and output constraints. IEEE Control Syst Lett 2021;5(1):343–8. http://dx.doi.org/10.1109/LCSYS.2020.3002152.

[30] Ortmann L, Hauswirth A, Caduff I, Dörfler F, Bolognani S. Experimental validation of feedback optimization in power distribution grids. Electr Power Syst Res 2020;189(106782). http://dx.doi.org/10.1016/j.epsr.2020.106782.

[31] Bertsekas DP. Constrained optimization and lagrange multiplier methods (Optimization and neural computation series). Athena Scientific; 1996.

[32] Ruszczynski A. Nonlinear optimization. Princeton University Press; 2011.

[33] Tan Y, Chen Y, Li Y, Cao Y. Linearizing power flow model: A hybrid physical model-driven and data-driven approach. IEEE Trans Power Syst 2020;35(3):2475–8. http://dx.doi.org/10.1109/TPWRS.2020.2975455.

[34] López-Erauskin R, González A, Petrone G, Spagnuolo G, Gyselinck J. Multivariable perturb and observe algorithm for grid-tied PV systems with joint central and distributed MPPT configuration. IEEE Trans Sustain Energy 2021;12(1):360–7. http://dx.doi.org/10.1109/TSTE.2020.2996089.

[35] Xiao-Kang L, Yan-Wu W, Pengfeng L, Peng W. Distributed supervisory secondary control for a DC microgrid. IEEE Trans Energy Convers 2020;35(4):1736–46. http://dx.doi.org/10.1109/TEC.2020.2994251.

[36] Strunz K, et al. Benchmark systems for network integration of renewable and distributed energy resources. In: CIGRE task force C6.04.02. 2014, p. 119.